

Physics-based Reflectance Estimation Applied To Recoloring

Shida Beigpour

SHIDA@CVC.UAB.ES

Computer Vision Center/Computer Science Department

Building O - Campus UAB, 08193 Bellaterra (Barcelona), Spain

Advisor: Joost van de Weijer

Abstract

Recoloring is a term referring to alteration the color of an object in an image. We propose a new method where a physics-based surface reflectance estimation has been utilized for modeling the change in the chromaticity of an object and illuminant light. Unlike the existing methods, chromaticity of an object is estimated independent of the illuminant. This report presents a novel approach where the illuminant color is estimated from a single surface without any further assumption on the chromaticity of the illuminant. Realistic recoloring results achieved on complex natural images captured by uncalibrated cameras clearly demonstrate that the proposed framework significantly outperforms state-of-the-art work on recoloring which disregards the underlying rules of physics.

Keywords: Dichromatic Reflection Model, Physic-based vision, Color-vision, Recoloring

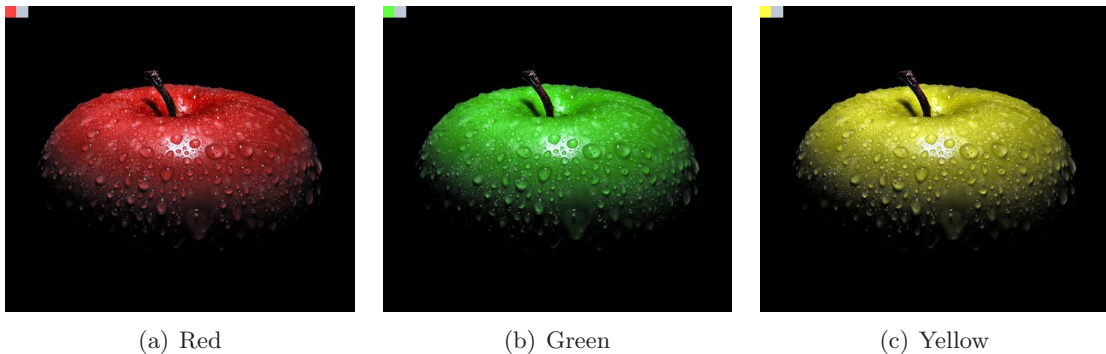


Figure 1: A snapshot of an apple has been recolored with two different colors using our method. Can you guess which one is the original photograph?!

Contents

| | | |
|----------|--|-----------|
| 1 | Introduction | 3 |
| 2 | Related work | 4 |
| 2.1 | Colorization and recoloring | 4 |
| 2.2 | Physics-based Methods | 6 |
| 3 | Physic-based Color Modeling and Recoloring | 7 |
| 3.1 | Dichromatic Reflection Model (DRM) | 7 |
| 3.2 | Intrinsic images estimation | 8 |
| 3.3 | Color alteration or Recoloring | 9 |
| 4 | Chromaticity estimation methods | 10 |
| 4.1 | Dichromatic plane estimation | 11 |
| 4.2 | Body reflectance color estimation | 11 |
| 4.3 | Illuminant chromaticity estimation | 13 |
| 4.3.1 | Confined illuminants estimation (CIE) | 14 |
| 4.3.2 | Unrestricted illuminants estimation (UIE) | 15 |
| 5 | Results | 16 |
| 5.1 | Evaluating the methods using synthetic images | 17 |
| 5.2 | Recoloring of natural images | 19 |
| 5.3 | UIE method on natural images | 19 |
| 5.4 | Preliminary results on handling interreflections | 22 |
| 6 | Conclusion and Future Work | 22 |

1. Introduction

Colorization is a term introduced by Wilson Markle in 1970 to describe the computer-assisted process he invented for adding color to black and white classical movies, TV programs and old images (Burns). Several commercial applications and plug-ins have been developed to facilitate this task so far (Markle, 1984). Obtaining a color image from grayscale is a very ill-posed problem; therefore conventional methods require intensive user-interaction that is given a set of color hints estimated by a human operator, a colorization method applies these colors to the grayscale image in order to obtain a color image similar to what the original scene could be like (Levin et al., 2004). Note that the result would be highly dependent on user’s choice of colors. Movie colorization is often achieved by tracking pixels in each frame, and applying the color from their corresponding pixel in the first colored frame (Martinez and Lim, Jun 13, 1989). The main problem of colorization methods, despite their high computational cost, is that as they are only dealing with gray-scale images, their application is limited to old images, and movie frames.

Recoloring or color-alteration, on the other hand, is a term referring to the modification and adjustment of the image color appearance. Color modification methods are applied to photo montage (Lalonde et al., 2007), color correction, visual effects in movies (Reinhard et al., 2004), and also in industrial and commercial applications as a technique to visualize the final color appearance of the 3D object products before actual production in order to improve and facilitate their design (Shen and Xin, 2005). In this report we will focus on recoloring an object in a single snapshot.

Some *graphical* methods have been developed for colorization and recoloring so far in which the colors are being shifted or propagated through the image using complex mathematical equations. Graphical methods often fail to properly generate a realistic perception of the recolored object (e.g. the case of non-white illuminant) as they suffer from a lack of knowledge about the physics behind it. One would raise an important question: “*What makes an object look realistic in an image?*”. This question can be answered with the help of physics rules applied on the light interaction with the object surface. In that way, we come to the realization that, the incident light not only affects the brightness of the pixels we perceive in the image of an object, but also affects their chromaticity. Therefore we believe by making a distinction between different regions of the object surface (e.g. shading, and highlights), and decomposing the object chromaticity into the natural color of the object surface as well as the color of the illuminant, we are capable of performing the correct color modification.

To this end, we have developed a physics-based method that not only is capable of incorporating all the 3 channels of a high quality photo, but also results in a high quality re-colored image by extracting the physic-based geometrical model of the light interaction with the object surface. This physic-based model, known as the *Dichromatic Reflection Model (DRM)* (Section 3.1), is capable of interpreting the object-pixel color-values in the image resulting in the geometrical models of the object surface reflectance and the incident light (known as the *intrinsic images*). Yet we have managed to maintain a fairly low computational cost and, with the exception of object segmentation, virtually no user interaction

is required. Unlike most coloring methods, we don't require to convert the image to a color space other than RGB.

Realistic results achieved through experiments clearly demonstrate that the proposed framework significantly outperforms previous work on recoloring in which the underlying physics rules have been disregarded. The existing methods based on physics-based reflectance model have only presented results for a set of images taken under laboratory restricted conditions. To best of our knowledge, we have obtained the first reported results for reflectance estimation in real-world images with complex shading and highlights.

The rest of the report is organized as follows: First a review of the related work is given in Section 2. Then our main goal is discussed in Section 3; followed in Section 4 by the detailed explanation of the method we have developed to solve the problem. Section 5 analyzes the results we have obtained. Conclusions are drawn in Section 6 followed by ideas for improving the performance of the method in our future work.

2. Related work

Even though the image colorization trend dates back to 70s, color modification recently has attracted much attention as the quality of the imaging devices has been improved. Color modification in an image is an active research in computer vision as well as computer graphics. Several methods have been developed so far in order to improve the quality of the result, speed up the process, and decrease the user assistance as much as possible. We first review the methods dealing with color modification which would include: colorization applied to recoloring, color shifting, and color transfer between images. Later on in this section, we investigate the state-of-the-art dealing with reflectance estimation.

2.1 Colorization and recoloring

Several methods developed for colorization of the gray-scale snapshots have also been used in order to modify a colored image. These methods mainly consist of partial hand-coloring of regions of an image or video and propagating the colored points (known as *color markers* or *hot-spots*) to the rest of the image using a fairly complex optimization algorithm. Examples of such optimizations in existing literature include: *energy* (the difference of neighboring pixels brightness) minimization (Konushin and Vezhnevets, 2006) which is inspired by graph-cut algorithm (Vezhnevets, 2005), and color similarity maximization of neighboring pixels in space-time that have similar intensities (Levin et al., 2004). The main problem with such methods is their significant computational time as well as excluding the color information obtained by modern imaging devices. Both above mentioned methods work solely in YUV color-space. Color-marker based methods are often incapable of achieving high quality results and preserving the sharp texture as they perform a zero-order color approximation of the object. The intensive user assistance to assign the markers needs to be repeated as well as the entire computation every time the choice of color changes. The main advantage of such methods is that no segmentation is required and the colorization can be performed for multiple objects in the scene with different colors simultaneously.

To improve the result of the existing color-marker based colorization, a novel method has been developed based on the idea that preserving the image contrast results in a more

realistic colorization. In this method, the result of a color-marker based colorization is then adjusted so that the direction of the maximum-contrast would agree with the gradient in the original gray image (Drew and Finlayson, 2008). The authors have expressed that although the color values specified by the markers as well as the pixel-wise brightness would not necessarily be preserved, a fairly realistic colorization has been achieved. Despite the significant improvement in the quality of the colorization result, the method still suffers from some of the main drawbacks of the marker-based colorization methods used as its prior stage. In fact the computational complexity has even been increased, while the application of the method is still limited to gray-scale images. However, the amount of user-interaction is partially decreased as the method can better handle complex shading and color-contrast without the detailed marker-specification required by previous methods.

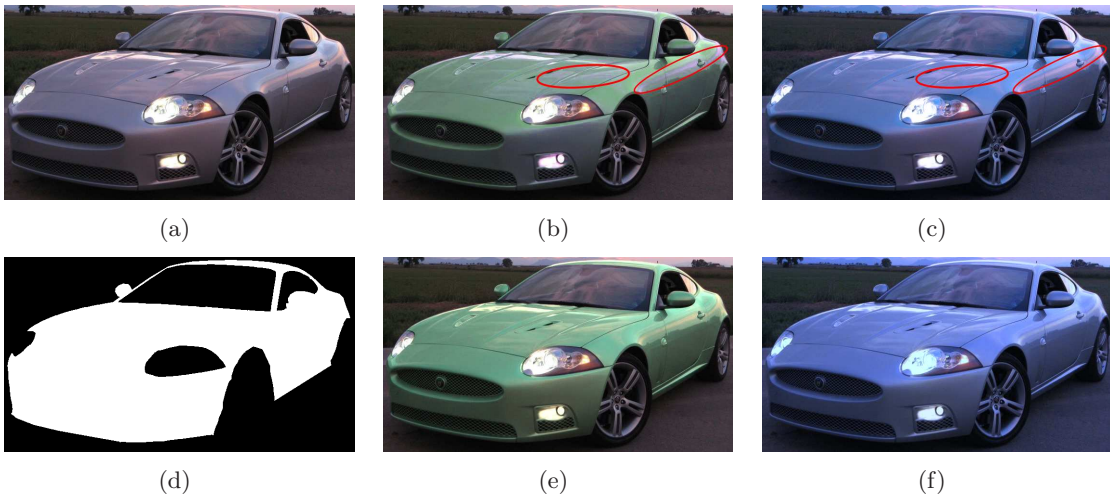


Figure 2: Here the effect of developing a physical reflection model is demonstrated: (a) The original image; (d) Segmentation mask; (b)and(c) are the results of recoloring and applying cooling photo filter respectively using a professional photo-editing software which fails to handle areas of highlights (errors are marked in red); (e)and (f) have been obtained by proposed method in which the areas of highlights are treated differently than the rest of the object surface.

Color modification and recoloring algorithms embedded in professional photo-editing applications perform by calculating an offset in the hue, saturation and luminance between the source and destination colors. The source image is then adjusted using these offsets to produce the desired color (Gonsalves, Feb 26, 2002). Such methods are often quite fast, yet they suffer from a lack of physical model to correctly separate object reflectance from illuminant color in the image leading to a less realistic result, while requiring a perfect prior segmentation for the object of interest. Figure 2 compares the recoloring result of a professional photo-editing application with the recoloring achieved by the proposed method, as the later seems to be more robust dealing with a non-white illuminant.

Recently another type of image color modification called *color transfer* has been introduced which is capable of extracting the color characteristics from a source image and applying it to a target image producing an image with the target scene but look and feel of the source image (e.g. warm-tone sunset). To address that goal, a method has been developed which decomposes the covariance between three components of pixel values while calculating the mean along each of the three axes, and then a transform is calculated to scale, rotate and shift pixel data of target image to fit to the color distribution of the source image (Xiao and Ma, 2006). In a very similar work, the color transfer process has been optimized to work in real-time (Reinhard et al., 2004). While the former method can perform in any color space, the later approach is restricted to $L\alpha\beta$ space. Both methods result in a fairly realistic modified image. However in the case of the source and target images being different in texture and characteristics to a great extent, a set of swatches is required to be specified by user which extends the user-interaction. Unlike color transfer, in recoloring tasks only a snapshot of an object is given, and often no information about the color distribution of the target scenes available.

2.2 Physics-based Methods

Object reflectance estimation from an image is an active subject in color-vision whose application ranges from color constancy to segmentation and classification. The main idea is if we would be able to build a realistic model of the light interaction with the object surface, we could extract crucial knowledge about the object surface geometry as well as the illuminant light. Such knowledge would then be used in order to remove the effect of a non-white illumination (*color constancy*), locate and remove the areas of shadows and highlights (essential in *object segmentation*), and obtain the geometrical model of the object (improving the *object classification*). Therefore the followings is devoted to a review on methods in which an understanding of the physics behind the object color perception is developed based on the *Dichromatic Reflection Model (DRM)* which will be explained in more details in Section 3.1.

Using the idea that the main variations in an image sequence of a fairly static outdoor scene should be the illumination changes, a method for object color decomposition has been developed in which the object surface reflectance model has been extracted, assuming the camera response to be linear (Weiss, 2001). The author has used the assumption that when derivative filters are applied to natural images, the filter output tend to be sparse. Then a maximum likelihood estimator has been used for surface reflectance recovery.

A novel approach has been developed for color transfer with the assumption of known illuminant. First a DRM is fitted to the object pixels in order to decompose the object pixel values to global object chromaticity and its geometrical model, but to avoid over-fitting, the model is optimized not only in regard to the source color, but also to the desired target color (Shen and Xin, 2005). Therefore, the main innovation in this method is exploiting a weighted least square giving more importance to the color channels whose source and target values are more different. In order to estimate the source object color, the authors suggested to use the pixels whose color vector angle to illuminant color vector is greater. The DRM fitting have also been used for the matter of color-based segmentation. Interesting results have been obtained using this method; however the extracted geometrical model of the

object is dependent on the target, and the problem of unknown illuminant is yet to be solved.

3. Physic-based Color Modeling and Recoloring

In order to develop a better understanding of the light interaction with the object surface, we use a physics-based model of reflection called the *Dichromatic Reflection Model* (Shafer and Lischinski, 1985) which enables us to extract the knowledge necessary for modeling the effect of changes in the illuminant and object colors on the object perception. This model states that two distinct types of reflection -body and interface reflection- occur, and that each type can be decomposed into a relative spectral distribution and a geometric scale factor. Therefore given an image of an object in any imaging conditions, as long as our assumptions hold, we are capable of extracting the geometrical characteristics of that object and the illuminant light. These geometrical characteristics would then enable us to generate a snapshot of that object with the same imaging condition varying only the chromaticity of the object and illuminant light.

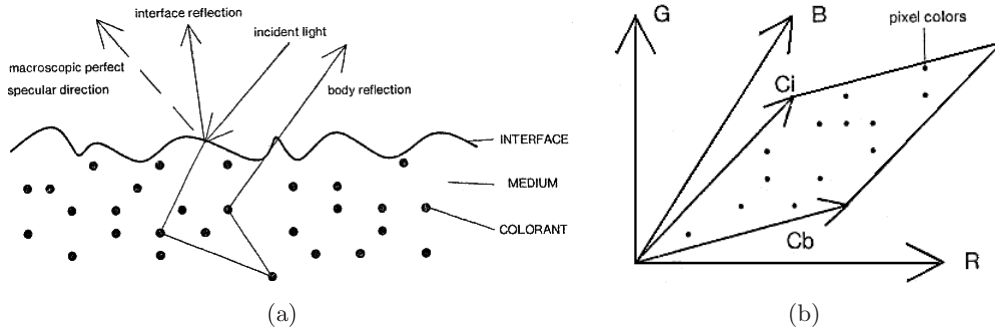


Figure 3: (a) Reflection of the light from an inhomogeneous material; (b) Pixel values for a set of points on a single surface lie within a parallelogram in color space.

3.1 Dichromatic Reflection Model (DRM)

According to Shafer, pixel values for a set of points on a single surface must lie within a parallelogram in the RGB space, bounded by RGB vectors \mathbf{C}_i and \mathbf{C}_b (here on we indicate vectors in bold font). These vectors represent the direction of the interface and body reflectance from the object surface respectively (Figure 3(b)). The validity of the dichromatic model has been proven for a variety of inhomogeneous dielectric materials commonly observed in natural scenes (Tominaga and Wandell, 1989). Although this model does not assume a point light or uniform illumination distribution over the scene, it requires a prior segmentation (Figure 4(b)) for multi-colored objects in order to fulfill the assumptions of the model.

The dichromatic model can describe the color of each pixel inside a single-colored object and illuminated by a single-colored illuminant, using images of the amount of body ("dif-

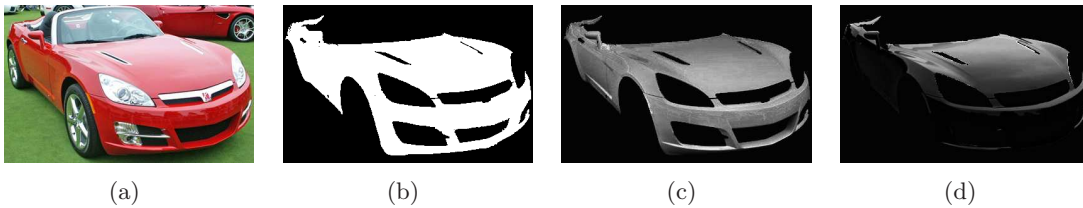


Figure 4: Here the DRM fitting have been applied on a natural image with complex shading and highlights: (a) The original image; (b) Segmentation mask; (c) and (d) are the intrinsic images for body and interface reflectances respectively.

fuse”) and interface (*specular*”) reflections at each pixel which are called *intrinsic* images (Figure4(c) and 4(d)). Equation 1 demonstrates the dichromatic model in the mathematical format, where \mathbf{f} is the RGB triple defining the color of every pixel in the object surface, m_b and m_i are the intrinsic images of body and interface reflectance respectively, and \mathbf{C}_b and \mathbf{C}_i are the colors of the corresponding colors.

$$\mathbf{f} = m_b \mathbf{C}_b + m_i \mathbf{C}_i \quad (1)$$

Several methods have been developed to approximate the dichromatic model of an object. Kravtchenko and Little have introduced a spatial-based approach in their segmentation method in which they approximate the two dichromatic planes for specular and body reflectance considering the lighter and darker pixels separately (Kravtchenko and Little, 1999). Shen and Xin have solved the model with the assumption of a known illuminant (Shen and Xin, 2005). Later on we propose a novel method in which a fairly accurate approximation of the dichromatic plane of an object under an unknown illuminant is achieved.

3.2 Intrinsic images estimation

Using the correlated RGB color space the dichromatic equation can be solved with the assumption that the \mathbf{C}_b and \mathbf{C}_i color vectors are constant for the entire object to be re-colored (single-colored object and illuminant). The material coefficients (m_b and m_i) are fixed for each pixel which means the coefficients are the same for R, G, and B values of the same pixel. Then for an image of N pixels, we would have $3 \times N$ equations (Equation 2) while the number of unknown values would be $2 \times N$ for m_b and m_i in addition to the 6 values defining the RGB triples of \mathbf{C}_b and \mathbf{C}_i color vectors. Having said that, for a large enough number of pixels, this set of equations can then be solved using an error minimization. Algorithms for approximating \mathbf{C}_b and \mathbf{C}_i are proposed in section 4

$$\begin{pmatrix} R_j \\ G_j \\ B_j \end{pmatrix} = m_{b_j} \times \begin{pmatrix} C_b^R \\ C_b^G \\ C_b^B \end{pmatrix} + m_{i_j} \times \begin{pmatrix} C_i^R \\ C_i^G \\ C_i^B \end{pmatrix} \quad (2)$$

Therefore, given the RGB values of \mathbf{C}_b and \mathbf{C}_i , and using the pixel RGB values \mathbf{f} , we are able to calculate the intrinsic image matrices m_b and m_i which minimize the fitting error of

the model to the object pixels. In other words, given the dichromatic plane defined by \mathbf{C}_b and \mathbf{C}_i we extract the geometrical model of body and specular reflectance by minimizing the projection error of object pixel value on the plane (Equation 3). Note that the pseudo-inverse notation implies the least square error minimization.

$$\mathbf{f} = \begin{bmatrix} C_b^R & C_i^R \\ C_b^G & C_i^G \\ C_b^B & C_i^B \end{bmatrix} \times \begin{bmatrix} m_b \\ m_i \end{bmatrix}$$

$$\begin{bmatrix} m_b \\ m_i \end{bmatrix} = \text{pinv} \left(\begin{bmatrix} C_b^R & C_i^R \\ C_b^G & C_i^G \\ C_b^B & C_i^B \end{bmatrix} \right) \times \mathbf{f} \quad (3)$$

The correlated RGB color space and Gamma Correction

RGB is a common color space for monitors and is more convenient for users. But since it is a *correlated* color space, most existing coloring methods require a transformation of image pixels into a non-correlated and more photometric invariant color space in order to "*decorrelate*" the color (Reinhard et al., 2001). In contrast, we do not require any decorrelation transform. Using the RGB color space one should bear in mind that due to the *Gamma expansion* that occurs largely in the nonlinearity of the electron-gun current-voltage curve in Cathode Ray Tube (CRT) monitor systems, image signals are *gamma encoded* (Equation 4) prior to be shown on monitors which helps to map signals into a more perceptually uniform domain (Poynton, 2003). Therefore a *Gamma Correction or decoding* (Equation 5) process should be performed on the image signals to preserve the linearity of the color signals prior to the DRM approximation.

$$V_{out} = V_{in}^\gamma \quad (4)$$

$$V_{out} = V_{in}^{\frac{1}{\gamma}} \quad (5)$$

In this thesis we use images from the Internet for which no calibration data is available. For that matter we have set γ to be 2.2 for sRGB color space.

3.3 Color alteration or Recoloring

The main goal of our method is changing both object and illuminant colors. After the estimation of the object reflectance model, recoloring of the object is straightforward. The entire color alteration process is demonstrated in the Equation 6, where \mathbf{f}' is the object reflectance in the new body and illuminant color (\mathbf{C}_b' and \mathbf{C}_i' respectively) specified by the user.

$$\mathbf{f}' = m_b \times \alpha \times \mathbf{C}_b'' + m_i \times \mathbf{C}_i' \quad (6)$$

$$\mathbf{C}_b'' = \begin{bmatrix} C_i^{R'}/C_i^R & 0 & 0 \\ 0 & C_i^{G'}/C_i^G & 0 \\ 0 & 0 & C_i^{B'}/C_i^B \end{bmatrix} \times \mathbf{C}_b' \quad (7)$$

Note that according to the model (see Figure 3(a)), the body reflectance itself relies also on the illuminant color. Therefore, we have modeled the effect of illuminant color changes on the object surface using the term \mathbf{C}_b'' which is defined as in Equation 7. We have introduced a new term α to simulate the desired change in the color intensity as the colors in the dichromatic model are normalized and due not account for intensity. For the case of multi-colored objects, different regions should be separated prior to recoloring in order to fulfill the DRM assumption of single-colored object while preserving the areas of highlights.

Note that despite the computational complexity of the dichromatic plane estimation, the re-coloring algorithm has been defined as simple as addition and multiplication operations which, implemented in logic-gates, would perform in real-time. This can be considered as a unique ability compared to most state-of-the-art methods which require to repeat their entire process each time a new color is specified.

4. Chromaticity estimation methods

In this section we propose methods for the estimation of the body reflectance color \mathbf{C}_b and interface reflectance color \mathbf{C}_i (Figure 5(c)). The body reflectance color (\mathbf{C}_b) is estimated using Robust Singular Value Decomposition (RSVD) regardless of illuminant color. Two approaches will be introduced in this section which are capable of estimating the illuminant color (\mathbf{C}_i).

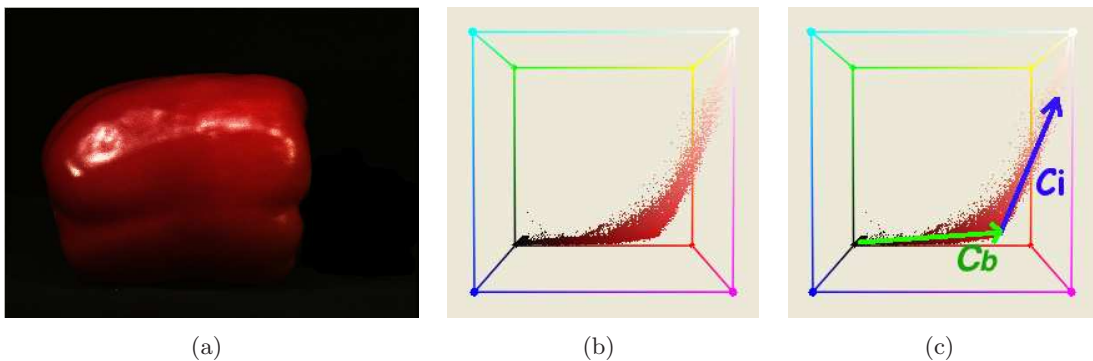


Figure 5: Color histogram for a single-colored object in the presence of highlights is demonstrated: (a) Original image; (b) RGB color histogram; (c) Expected directions for body and interface reflectance chromaticities are marked as \mathbf{C}_b and \mathbf{C}_i vectors;

4.1 Dichromatic plane estimation

In order to estimate the color vectors defining this parallelogram, first a plane is fitted to the object pixels. Consider a plane with a normal $\hat{\mathbf{n}}$. In the ideal case every object pixel should belong to the plane, but in practice, as we do not limit the imaging conditions and due to noise, not all pixels would fall in the plane. The projection error for a point $\mathbf{f}(\mathbf{x})$ of the object onto the plane would then be defined as the perpendicular distance from the pixel RGB vector to the plane:

$$e(\mathbf{x}) = \left\| (\mathbf{f}(\mathbf{x}))^T \hat{\mathbf{n}} \right\| \quad (8)$$

We use $\hat{\cdot}$ to indicate the unit length vectors. The total error for all points on the object (indicated by the region Ω) in the LS sense is

$$e = \int_{\Omega} e^2(\mathbf{x}) d\mathbf{x} = \int_{\Omega} \hat{\mathbf{n}}^T (\mathbf{f}\mathbf{f}^T) \hat{\mathbf{n}} d\mathbf{x} = \hat{\mathbf{n}}^T \mu \hat{\mathbf{n}} \quad (9)$$

where μ is the structure tensor. We use the Lagrange multiplier to model the constraint that $\hat{\mathbf{n}}^T \hat{\mathbf{n}} = \mathbf{1}$,

$$\lambda (1 - \hat{\mathbf{n}}^T \hat{\mathbf{n}}) + \hat{\mathbf{n}}^T \mu \hat{\mathbf{n}}. \quad (10)$$

This equation is minimized by setting the derivative to zero

$$\mu \hat{\mathbf{n}} = \lambda \hat{\mathbf{n}} \quad (11)$$

As expected, the minimal error is obtained by finding the eigenvector corresponding to the smallest eigenvalue of the distribution. Using the dichromatic plane, the search for the two chromaticity directions is limited to within a plane. We went through the steps of this derivation because it better explains the robust extension which follows below. Note that this steps would also be helpful in Section 4.3.2.

4.2 Body reflectance color estimation

The object pixel values for which the $m_i = 0$ form a line passing through the origin. Fitting a line through these pixels allows us to compute \mathbf{C}_b . The fitting error of an object pixel to a line given by the vector $\hat{\mathbf{v}}$ is

$$e(\mathbf{x}) = \left\| \mathbf{f}(\mathbf{x}) - \left((\mathbf{f}(\mathbf{x}))^T \hat{\mathbf{v}} \right) \hat{\mathbf{v}} \right\| \quad (12)$$

And the total fitting error for all the pixels inside Ω is (we will omit the spatial arguments)

$$\int_{\Omega} e^2 d\mathbf{x} = \int_{\Omega} \mathbf{f}^T \mathbf{f} - \hat{\mathbf{v}}^T (\mathbf{f}^T \hat{\mathbf{v}})^T \mathbf{f} - \mathbf{f}^T (\mathbf{f}^T \hat{\mathbf{v}}) \hat{\mathbf{v}} + \hat{\mathbf{v}}^T (\hat{\mathbf{v}}^T \mathbf{f}) (\mathbf{f}^T \hat{\mathbf{v}}) \hat{\mathbf{v}} d\mathbf{x} \quad (13)$$

Using the constrain $\hat{\mathbf{v}}^T \hat{\mathbf{v}} = 1$ we have:

$$\hat{\mathbf{v}}^T (\hat{\mathbf{v}}^T \mathbf{f}) (\mathbf{f}^T \hat{\mathbf{v}}) \hat{\mathbf{v}} = \hat{\mathbf{v}}^T \mathbf{f} \mathbf{f}^T \hat{\mathbf{v}}$$

And it can be proven that:

$$\hat{\mathbf{v}}^T(\mathbf{f}^T\hat{\mathbf{v}})^T\mathbf{f} = \mathbf{f}^T(\mathbf{f}^T\hat{\mathbf{v}})\hat{\mathbf{v}} = \hat{\mathbf{v}}^T\mathbf{f}\mathbf{f}^T\hat{\mathbf{v}}$$

Therefore the error term (Equation 13) can be rewritten as:

$$e = \int_{\Omega} \mathbf{f}^T\mathbf{f} - \hat{\mathbf{v}}^T(\mathbf{f}\mathbf{f}^T)\hat{\mathbf{v}} d\mathbf{x} \quad (14)$$

The above equation can be solved in a similar way as in the previous section using the Lagrange multiplier and setting the derivative to zero. However the minus sign in the equation indicates that here the eigenvector which corresponds to the higher eigenvalue is desired. Intuitively, having the assumption that most of the object pixels belong to the body reflectance, the higher eigenvalue is expected to indicate the \mathbf{C}_b direction.

Robust Body Reflectance Estimation.

Although the least squares (LS) orientation estimation used in SVD would perform well in the case that all pixels belong to the same orientation, in our case, in which there are two main orientations (\mathbf{C}_b and \mathbf{C}_i), the LS estimation will mix the two orientations and give a wrong result. In order to avoid that, a *robust estimator* (van de Weijer and van den Boomgaard, 2005) is constructed:

$$e(\mathbf{x}) = \int_{\Omega} \rho(e(\mathbf{x}))d\mathbf{x} \quad (15)$$

In the current work we will apply the following *Gaussian error norm*:

$$\rho(e) = 1 - \exp\left(-\frac{e^2}{2m^2}\right) \quad (16)$$

In a robust estimator, large deviations from the model are considered as outliers, and therefore, they are not taken into account very heavily. While LS estimation is very sensitive to outliers. In our application large deviations from the model are mainly due to the mixing of two different directions, \mathbf{C}_b and \mathbf{C}_i . The error, Equation 15, can now be rewritten as (we will omit the spatial arguments):

$$e = \int_{\Omega} \rho\left(\sqrt{\mathbf{f}^T\mathbf{f} - \hat{\mathbf{v}}^T(\mathbf{f}\mathbf{f}^T)\hat{\mathbf{v}}}\right) d\mathbf{x} \quad (17)$$

Similar to Equation 10, a Lagrange multiplier is then used for minimization subject to the constraint $v^T v = 1$,

$$\frac{d}{d\hat{\mathbf{v}}}\left(\lambda(1 - \hat{\mathbf{v}}^T\hat{\mathbf{v}}) + \int_{\Omega} \rho\left(\sqrt{\mathbf{f}^T\mathbf{f} - \hat{\mathbf{v}}^T(\mathbf{f}\mathbf{f}^T)\hat{\mathbf{v}}}\right) d\mathbf{x}\right) = 0 \quad (18)$$

Using Equation 18, as the error function leads to

$$\eta(\hat{\mathbf{v}})\mathbf{v} = \lambda\hat{\mathbf{v}} \quad (19)$$

Where η is defined as follows and G^m is the Gaussian function at scale m .

$$\eta(\hat{\mathbf{v}}) = \int_{\Omega} \mathbf{f}\mathbf{f}^T G^m \left(\sqrt{\mathbf{f}^T\mathbf{f} - \hat{\mathbf{v}}^T(\mathbf{f}\mathbf{f}^T)\hat{\mathbf{v}}} \right) d\mathbf{x} \quad (20)$$

The main difference with the ordinary LS estimator is that here the matrix η is dependent on \hat{v} . Note that η is called "robustified" structure tensor in which the contribution of each object pixel vector is weighted not only by its distance to the plane, but also according to its distance to the orientation model. Again, points far away from the line direction $\hat{\mathbf{v}}$ are considered outliers, and therefore, do not corrupt the estimation.

A *fixed point* iteration scheme is used to find a solution. Let $\hat{\mathbf{v}}^i$ be the orientation vector estimate after i iterations. The estimate is then updated as the eigenvector $\hat{\mathbf{v}}^{i+1}$ of the matrix $\eta(\hat{\mathbf{v}}^i)$ corresponding to the largest eigenvalue, i.e. we solve the Equation 21. The proposed scheme is a generalization of the well-known fixed point scheme (also called *functional iteration*) to find a solution of the equation $\hat{\mathbf{v}} = F(\hat{\mathbf{v}})$.

$$\eta(\hat{\mathbf{v}}^i)\hat{\mathbf{v}}^{i+1} = \lambda\hat{\mathbf{v}}^{i+1} \quad (21)$$

It should be noted that this iteration scheme is very similar to mean-shift, bilateral filtering, and anisotropic diffusion (van den Boomgaard and van de Weijer, 2002). Figure 6 illustrates an example of the iterative search for direction of the \mathbf{C}_b . The original estimation made by ordinary LS is refined at each iteration by changing the weights leading the method to converge to the robust, and in this case much better, estimation of the \mathbf{C}_b .

We need an initialization vector $\hat{\mathbf{v}}^0$ for the iterations which can prove crucial to estimation of the vector to which the algorithm would converge. Therefore, based on the fact that the specularities are brighter than the body reflectance pixels, instead of using all the pixels, we have decided to use the direction specified by the darker half of the object pixels as the initialization state to better guide the algorithm. While for the rest of the iterations we keep fitting and refining the model using the entire pixel set as the weightings in the robust estimation would already take care of the outliers.

Note that the iterative scheme does not necessarily lead to the *global* minimum of error. In fact, here we are not interested in that global minimum as the specular pixels are distributed along \mathbf{C}_i direction, while here we are only modeling the body reflectance chromaticity. And the specular pixels perform as a sort of outliers which our iterative refining algorithm is developed to decrease their effect on the \mathbf{C}_b estimation at each iteration.

4.3 Illuminant chromaticity estimation

In order to estimate the chromaticity of the illuminant (\mathbf{C}_i) two approaches were developed. The first illuminant estimation approach is based on the assumption that the colors which typical light sources display are limited to a set of standard illuminant, while the second

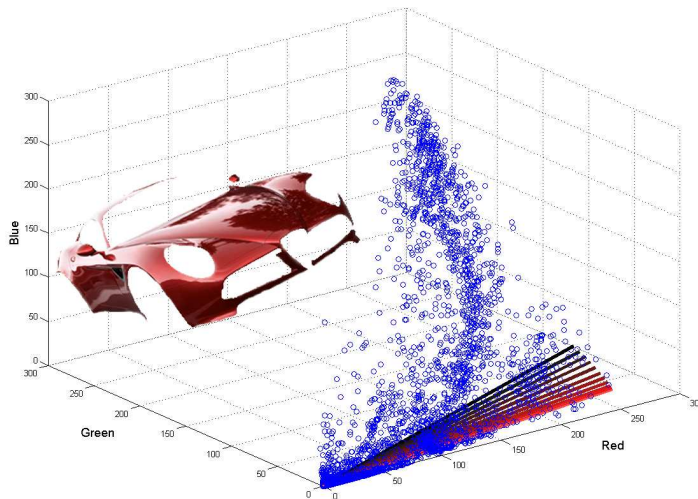


Figure 6: Here an example of robust body reflectance estimation is given. The primary estimation vector using ordinary SVD is demonstrated by black line, while the method iteratively converges to the robust estimation (marked in light red).

approach, can better deal with the case for which these assumption does not hold. The first approach is more robust to noise and doesn't require a fairly large specular area, whereas the second approach is fast and is capable of estimating non-planckian illuminants.

Several illuminant estimation methods have been proposed in *color constancy* research. To our knowledge, we present the first illuminant estimation based on the reflectance of a single-colored object. However in contrast to other methods we require a pre-segmented object. This problem can be overcome using a physics-based segmentation method (Vazquez et al., 2008). Note that for illuminant estimation, the segmentation is not required to be perfect.

4.3.1 CONFINED ILLUMINANTS ESTIMATION (CIE)

For the matter of simplification here in this approach we assume that the chromaticity of common light sources is limited and follows closely the Planckian locus of black-body radiators which is believed to be a function of temperature T in Kelvins (Finlayson and Schaefer, 2002). For this matter we sample the colors of the Planckian Locus (Figure 7) for the standard illuminants ($T \subset 4000 \sim 25000$ with steps of $1000 K^\circ$). Then the dichromatic equation is solved for all the pixels of the colored object using each of the possible illuminants, and m_b and m_i values are calculated. The illuminant chromaticity (\mathbf{C}_i) which minimizes the object reconstruction error (Equation 22) would be chosen, and the corresponding m_i and m_b values for each pixel are then considered as the dichromatic model of the object.

$$E(\mathbf{C}_b, \mathbf{C}_i) = \sum_j ((\mathbf{f}_j - m_{b_j} \mathbf{C}_b - m_{i_j} \mathbf{C}_i)^T (\mathbf{f}_j - m_{b_j} \mathbf{C}_b - m_{i_j} \mathbf{C}_i)) \quad (22)$$

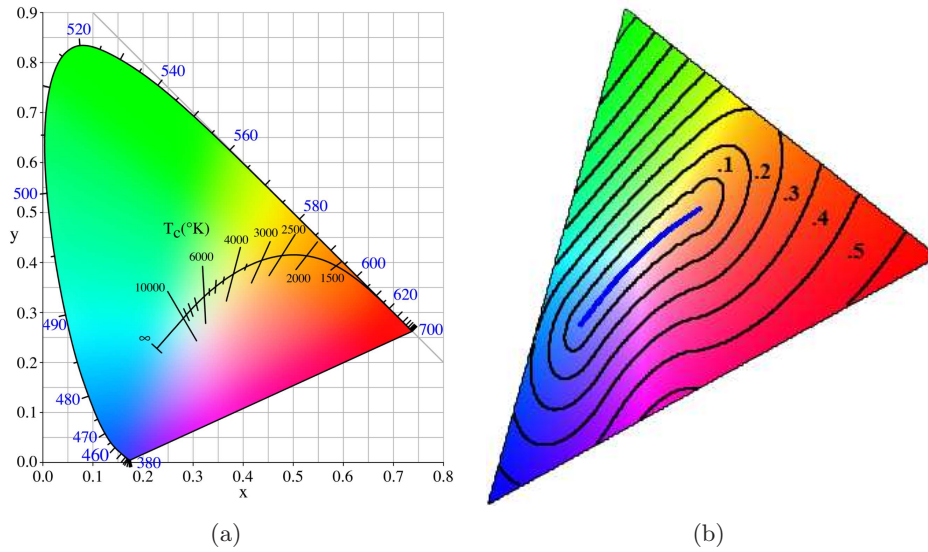


Figure 7: The chromaticity of common light sources is limited and follows closely the Planckian locus of black-body radiators: (a) The Planckian Locus inside the color gamut for CIE XYZ color space; (b) Color regions for which the distance to the Planckian Locus (sampled for T value of 4000~2500 degree Kelvin) are in the same range.

4.3.2 UNRESTRICTED ILLUMINANTS ESTIMATION (UIE)

In Section 4.3.1 we made an assumption of the Planckian illuminant in order to simplify the illuminant chromaticity estimation, here we solve a more general case in which this assumption would not hold. But as we no longer limit the range of the illuminant chromaticity, we require to collect enough information from the object surface in order to estimate the illuminant color. Therefore, we require the additional assumption of having a substantial number of object pixels falling into specular areas.

From our initial assumption of *single-colored* object, it follows that the variations in the chromaticity of the object surface can only belong to shading and highlights. We have further observed that most variations are caused by a single physical cause. Either the shape of the object causes the pixels to vary along \mathbf{C}_b or highlights cause them to vary along \mathbf{C}_i . Therefore, we make use of object pixels gradient in RGB-space, denoted by $\nabla \mathbf{f}$, to discover the orientation of these variations.

$$\nabla \mathbf{f} = \begin{pmatrix} R_x \\ G_x \\ B_x \end{pmatrix} \quad (23)$$

Here we apply the constraint of dichromatic plane by projecting the gradient vectors on the dichromatic plane using the eigenvectors corresponding to the highest calculated eigen-

values one being $\hat{\mathbf{v}}$ (the \mathbf{C}_b estimate from Section 4.2) and the other is the perpendicular vector which we call \mathbf{C}_1 . Therefore, we denote $\nabla\mathbf{f}_p$ as the projection of $\nabla\mathbf{f}$ onto the plane.

$$\nabla\mathbf{f}_p = (\mathbf{f}^T \cdot \mathbf{C}_b \quad \mathbf{f}^T \cdot \mathbf{C}_1)^T \quad (24)$$

The energy function $e_v(\alpha)$ is then defined as below:

$$e_v(\alpha) = \int_{\Omega} (\|\nabla\mathbf{f}_p(\mathbf{x})\|)^2 \delta(\alpha, \langle \hat{\mathbf{v}}, \nabla\mathbf{f}_p(\mathbf{x}) \rangle) d\mathbf{x} \quad (25)$$

Where $\langle \hat{a}, \vec{b} \rangle$ is the angle of vector \vec{b} to the direction \hat{a} , and $\delta(\alpha, \varphi)$ is defined as below:

$$\delta(\alpha, \varphi) = \begin{cases} 1 & |\varphi - \alpha| < T \\ 0 & \text{Otherwise} \end{cases} \quad (26)$$

Where T is the angle threshold. In fact, $e_v(\alpha)$ indicates the summed derivative energy, $(\|\nabla\mathbf{f}_p(\mathbf{x})\|)^2$, of all derivatives in the range $\alpha \pm T$.

Examples of the discrete histogram of gradients for three different objects are demonstrated in Figure 13. We chose $\hat{\mathbf{C}}_i$ as the direction whose angle to $\hat{\mathbf{C}}_b$ is α^i :

$$\alpha^i = \arg \max_{\alpha} e_v(\alpha) \quad (27)$$

As mentioned previously, the color variations on the single-colored object surface are due to either shading or highlights. We expect to observe up to two permanent peaks in the histogram. With the assumption of having substantial number of object pixels falling into specular areas, there should exist one peak in the histogram formed by the highlights. We observe two cases:

- Having only one peak in the histogram would indicate that the object surface is fairly smooth causing the shading derivative energy to be small, and therefore, the observed peak is due to highlights indicating the \mathbf{C}_i direction (Figure13(a)).
- In the case that two distinct peaks are observed, the peak with the highest absolute angle from \mathbf{C}_b direction indicates the \mathbf{C}_i direction (Figure13(b)). And the closest peak is around the \mathbf{C}_b direction.

5. Results

The main issue with analyzing the quality of a recoloring method is often lack of a proper groundtruth. Since little or no information regarding the pixel color distribution of the object with a different color or under a different illuminant in the real scene is available, the quality criteria of recoloring is subjective. In other words, the estimations can only be judged either using *reconstruction error*, or with the help of human users. Therefore, in order to evaluate the quality of our methods, we have made use of a set of synthetic images which enable us to introduce a *recoloring error* as well as a *chromaticity estimation error*. In this section, the two illuminant estimation methods have been compared using the before mentioned criteria and the more robust method has been selected and used for recoloring a set of natural images.

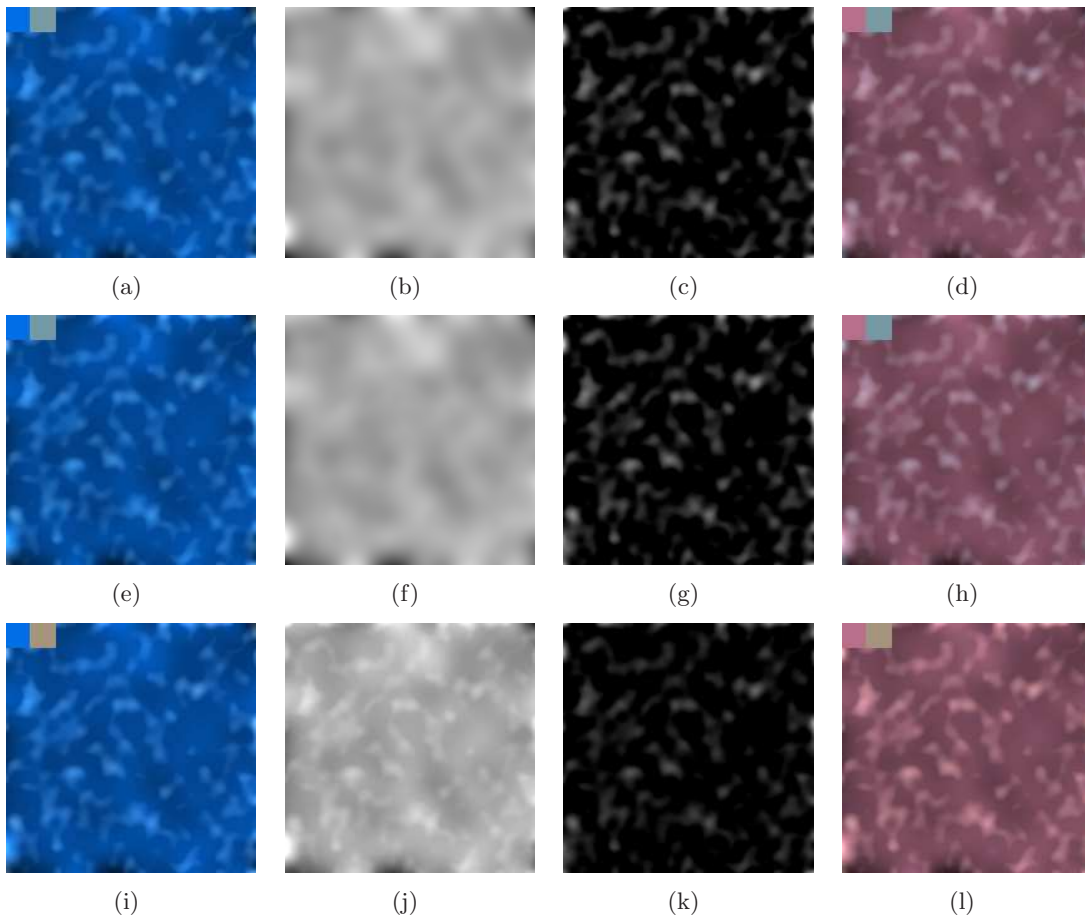


Figure 8: Two illuminant estimation methods have been compared using an example from the synthetic image dataset. (b) and (b) Examples of the intrinsic images (m_b and m_i) with which (a) and (d) has been generated; Given (a) to the methods: (f) and (g) are estimated intrinsic images using UIE; (j) and (k) are the estimated intrinsic images using CIE; (h) and (l) are generated using the estimated intrinsic image for each method with the same \mathbf{C}_b and \mathbf{C}_i as one producing (d). It's clear that the incorrect estimation using CIE have resulted in an incorrect recoloring.

5.1 Evaluating the methods using synthetic images

To evaluate the proposed chromaticity estimation methods, first a dataset of synthetic images has been generated which performs as a groundtruth for reflectance estimation and recoloring. The quality of the proposed chromaticity estimation methods is evaluated using two terms *Angular Estimation Error* and *Non-Planckianess* of the illuminant which are defined in this section.

SYNTHETIC IMAGE DATASET

The dataset of synthetic images (e.g, Figure8(a)) has been generated using 140 randomly generated RGB color vectors which are divided into two sets of the same size as \mathbf{C}_b and \mathbf{C}_i . For each pair of color vectors, \mathbf{C}_b and \mathbf{C}_i , a pair of low frequency noise images with different scales (Figure 8(b) and 8(c)) has been generated. Each synthetic image in the dataset has been generated by substituting these values in the DRM (Equation 1). The dataset consists of 4900 images. The process to generate each image is defined, in the mathematical notation, as follows. Let $B = \{\mathbf{C}_b^j : j = 1, \dots, |B|\}$ and $I = \{\mathbf{C}_i^k : k = 1, \dots, |I|\}$ be the sets of distinct color vectors for body reflectance and illuminant respectively. And for each pair of two color vectors \mathbf{C}_b^j and \mathbf{C}_i^k the matrices m_b^{jk} and m_i^{jk} are the randomly generated intrinsic images. Then each synthetic image \mathbf{img}^{jk} is:

$$\mathbf{img}^{jk} = m_b^{jk} \times \mathbf{C}_b^j + m_i^{jk} \times \mathbf{C}_i^k \quad (28)$$

ANGULAR ESTIMATION ERROR

The term *Angular Estimation Error (AEE)* is defined as the angle between the direction of the estimated and actual color vectors (\hat{V}_{est} and \hat{V} respectively) as defined in Equation 29. Here we report AEE in radians.

$$AEE = \arccos(\hat{\mathbf{V}} \cdot \hat{\mathbf{V}}_{est}) \quad (29)$$

NON-PLANCKIANNES

We define the term *Non-Planckianness (NP)* as the minimum angular distance of the light color vector $\hat{\mathbf{C}}_i$ to the Planckian locus in radians as given in Equation 30 where $\hat{P}(T)$ is the Planckian light vector for temperature value of T.

$$NP = \min\{\arccos(\hat{\mathbf{C}}_i \cdot \hat{\mathbf{P}}(\mathbf{T}))\} \quad (30)$$

The smaller NP values indicate the colors which are closer to the chromaticity of the natural illuminants. Figure 7(b) illustrates the illuminant colors for different NP values.

METHOD EVALUATION

As mentioned previously, for each image in the dataset, the chromaticity estimations have been performed using the three methods, and AEE has been used as a criteria to measure precision of the estimations. Here the Figure9(a) compares the measured angular estimation errors for each chromaticity estimation method based on the NP value of the illuminant. It is clear from the histogram that body reflectance color estimation is fairly independent of the NP of the illuminant light. As expected, for higher NPs, the UIE method out performs the CIE method.

The two illuminant estimation methods have also been compared using their *reconstruction error*(Figure9(b)) and mean *recoloring error*¹(Figure9(c)) demonstrating the robustness of UIE to the NP of the illuminant chromaticity. Note that although UIE is more robust,

1. *Recoloring error* for a synthetic image is defined as the mean square pixel-wise difference of the recolored images generated using the estimated and original intrinsic images. The mean is over the recoloring errors for an arbitrary set of \mathbf{C}_b and \mathbf{C}_i vectors (for that matter we have used 10 \mathbf{C}_b and 10 \mathbf{C}_i vectors).

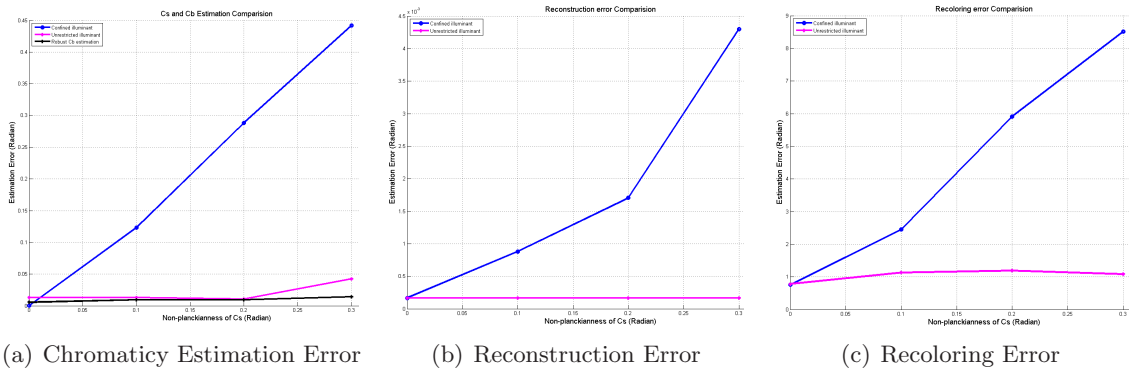


Figure 9: The chromaticity estimation methods have been compared using their angular estimation errors. Here the vertical axis represent the error value while the horizontal axis stands for the *Non-planckianness* of the illuminant light. The blue and magenta curves stand for measured errors using CIE and UIE illuminant estimation methods, while the black curve in Fig.(a) stands for *Angular Estimation Error* of the body reflectance chromaticity. Note that for the matter of recoloring and reconstruction the robust \mathbf{C}_b estimation method has been used along with the two \mathbf{C}_i estimation method.

CIE performs slightly better for estimating the illuminant in the case of a highly Planckian (natural) light which makes it competitive for images of the outdoor scenes.

5.2 Recoloring of natural images

A set of natural images have been recolored using our framework. We have chosen UIE method for illuminant estimation. The estimated intrinsic images are demonstrated in Figure10. The intrinsic images seem to make a good estimation of areas of highlights (see images of interface reflectance). Figure 11 and Figure 12 illustrate the results for illuminant and body reflectance changes respectively. Realistic results achieved suggest that the proposed framework outperforms previous work on recoloring in which the underlying physics rules have been disregarded.

Note that few existing methods which make use of physics-based reflectance model, have only presented the results on a set of images under laboratory restricted conditions (Shen and Xin, 2005). To best of our knowledge, these are the first reported results for reflectance estimation in real-world images with complex shading and highlights.

5.3 UIE method on natural images

In Section 4.3.2, two general types of the histogram of gradients (one or two major peaks) have been explained. In some natural images (e.g, 13(c)), We have observed a special case of the histogram with one major peak in which the peak has occurred very close to the \mathbf{C}_b direction, and therefore, the illuminant estimation method failed to make a realistic estimation of the illuminant color. We argue that this is due to the occurrence of the

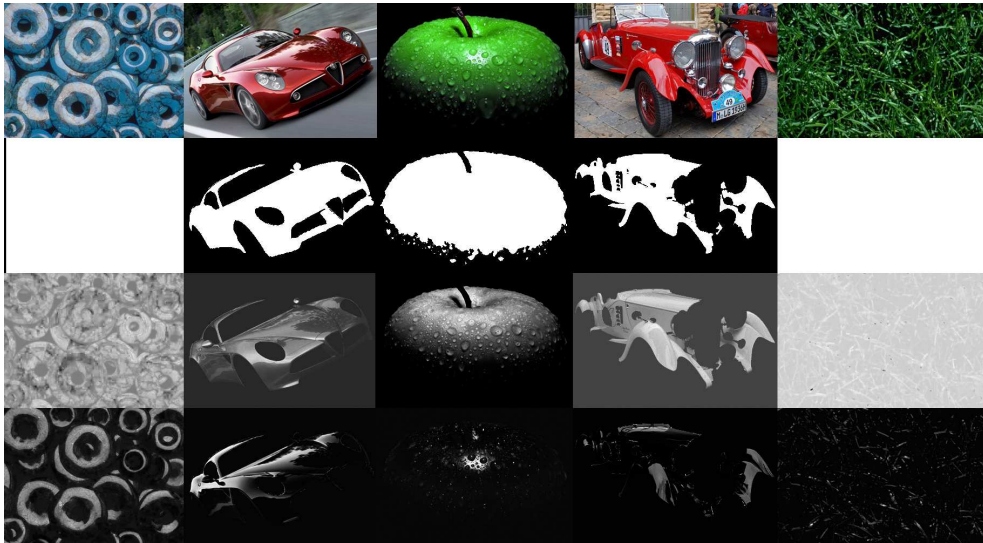


Figure 10: A set of natural images have been presented in the first row, followed, in the next rows, by the segmentation masks and the intrinsic images (m_b and m_i) obtained by our framework (with the option of UIE as illuminant estimation method). Note that for two cases, the entire image area has been used.

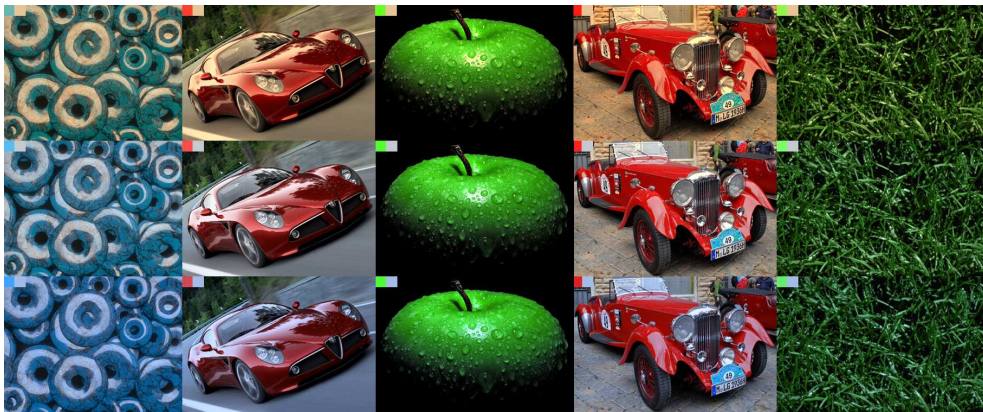


Figure 11: Here the result of changing illuminant chromaticity of the images presented in Figure10 using our framework has been presented. Each row obtained by setting the new \mathbf{C}_i to Planckian illuminant with the temperatures 4000, 7000, and 10000 Kelvin. Note that for the matter of visualization, we applied a simple color filter on the object surrounding to simulate the corresponding color composition.



Figure 12: Here the result of changing body reflectance chromaticity of the images presented in Figure 10 using our framework has been presented. The small squares at the top left of each image denote the user specified C_b with which the image have been obtained.

shading variations in the areas of the highlights which causes the direction indicated by pixel gradient to be a mixture of C_b and C_i . For that matter, we suggest the use of CIE method. Such experiments point out that further investigation of the gradient histogram is still required.

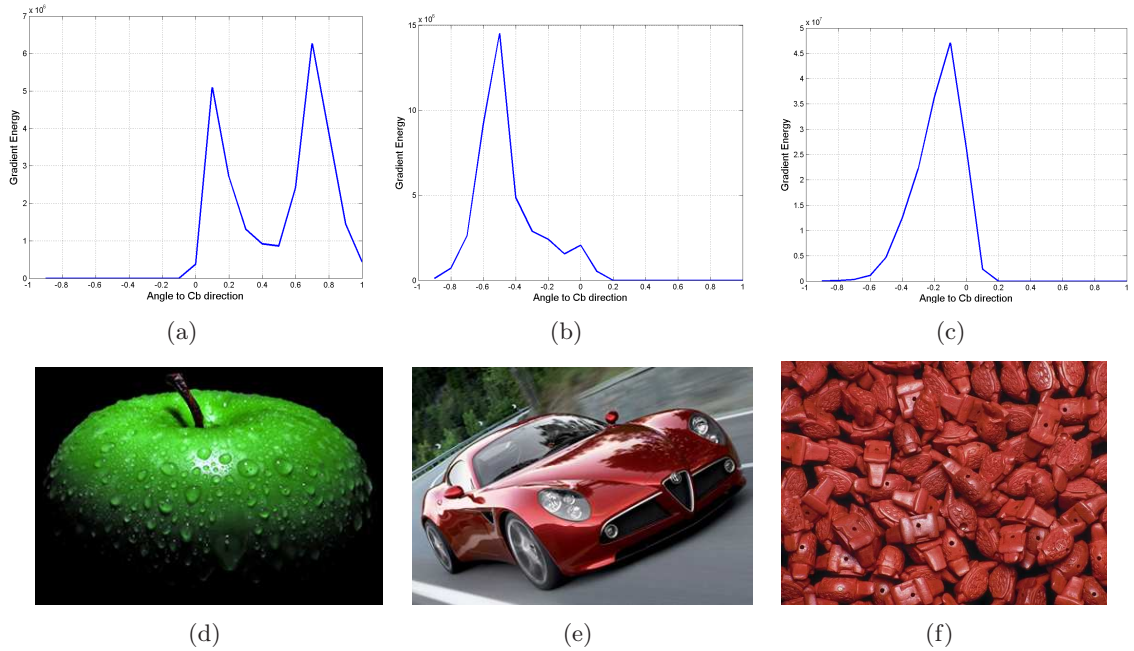


Figure 13: Examples of the discrete histogram of gradients for three different objects are presented: (a), (b), and (c) Illustrate the histograms; (d), (e), and (f) The original images.

5.4 Preliminary results on handling interreflections

Existence of interreflections of surrounding objects often makes the recoloring process much more complex, and the conventional photo-editing applications often fail to correctly model these details (Figure 14(b)). For our recoloring framework we have solved this problem based on the assumption that the area of interreflections is fairly small compared to the rest of the object, and would not affect the DRM estimation. Therefore, since our DRM fairly fits the object color vectors, the reconstruction error would be largely due to interreflections, and the difference between the original and the reconstructed images of the object would include the effect of the interreflections. Then simply by applying this difference image to the recolored image we preserve the interreflections. Figure 14 illustrates an example of area of interreflections along with the result given by a professional photo-editing software. Note that here the quality of the result is highly dependent on the accuracy of the estimated reflectance model.

6. Conclusion and Future Work

We have presented a physic-based method for the estimation of the object reflectance for presegmented images. The method simultaneously estimates the body and interface reflectances. Object chromaticity have been estimated independent of the illuminant color using a Robust SVD method. Two methods have been introduced in order to estimate the

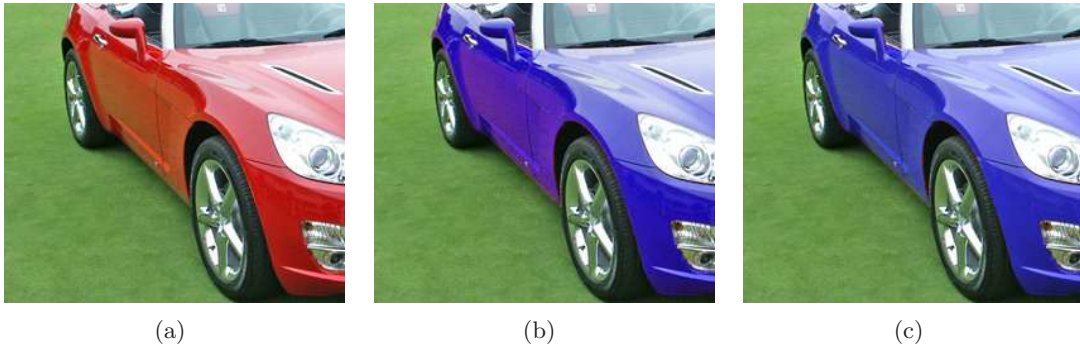


Figure 14: Preliminary results on handling interreflections (a) The original image; (b) The recoloring using a professional photo-editing software; (c) Recoloring obtained with our framework after including the interreflections.

chromaticity of the illuminant light. Using the proposed physic-based method a framework for modeling the change in the object color as well as the chromaticity of its illuminant light has been developed. The possible applications for this framework are photo montage, color correction, visual effects in movies, and also computer-aided design. The experimental results on natural images taken with non-calibrated cameras indicate that a realistic recoloring of an object with complex specularly and shading have been achieved. As the current framework is based on dichromatic reflection model, it requires the selected region to belong to a single-colored object under a single-colored illuminant, yet virtually no further user interaction is required. Finally we have managed to maintain a fairly low computational cost for reflectance estimation.

However, the current framework can be improved in several ways. We propose, as our future work, to embed into the framework an object segmentation method based on the Dichromatic Reflection Model. Also preliminary improvement of the estimations have been achieved by applying further restriction on the Dichromatic Reflection Model that is limiting the geometrical coefficients (intrinsic images) to positive values. In addition, it has been observed from the experimental results that when the illuminant and body reflectance chromaticities are close or complex shading variations occur in the areas of highlight, the estimation methods tend to confuse the actual chromaticities; therefore, further investigation on the estimation methods is required. Furthermore, we propose to make use of psychophysical experiments in order to introduce a quantitative measurement for the accuracy of the recoloring objects in the natural images. Lastly, we believe further investigation on handling colored shadows and interreflection on the object surface (especially the case in which chromaticity of the interreflections and object surface are close) may lead to a more robust recoloring framework.

References

- G. Burns. Colorization. museum of broadcast communications. Encyclopedia of Television.
- M.S. Drew and G.D. Finlayson. Realistic colorization via the structure tensor. ICIP, pages 457–460, Oct 2008.
- G. D. Finlayson and G. Schaefer. Solving for colour constancy using a constrained dichromatic reflection model. *International Journal of Computer Vision*, 42:127–144, 2002.
- R. Gonsalves. Method and apparatus for color manipulation. United State Patent 6,351,557, Feb 26, 2002.
- V. Konushin and V. Vezhnevets. Interactive image colorization and recoloring based on coupled map lattices. Graphicon’2006 conference proceedings, pages 231–234, July 2006. Novosibirsk Akademgorodok, Russia.
- V. Kravtchenko and J.J. Little. Efficient color object segmentation using the dichromatic reflection model. *Communications, Computers and Signal Processing, 1999 IEEE Pacific Rim Conference on*, pages 90 – 94, August 1999.
- J. F. Lalonde, D. Hoiem, A. A. Efros, C. Rother, J. Winn, and A. Criminisi. Photo clip art. In *SIGGRAPH ’07: ACM SIGGRAPH 2007 papers*, page 3, 2007.
- A. Levin, D. Lischinski, and Y. Weiss. Colorization using optimization. *SIGGRAPH ACM Transactions on Graphics (TOG) archive*, 23(3):689 – 694, August 2004. Special Issue: Proceedings of the 2004 SIGGRAPH Conference SESSION: Flash and color.
- W. Markle. The development and application of colorization. *SMPTE Journal*, pages 632–635, 1984.
- D. M. Martinez and J. S. Lim. Methods and apparatus for motion estimation in motion picture processing. United State Patent 4,838,685, Jun 13, 1989.
- Charles Poynton. *Digital Video and HDTV Algorithms and Interfaces*. 2003.
- E. Reinhard, M. Adhikhmin, B. Gooch, and P. Shirley. Color transfer between images. *Computer Graphics and Applications, IEEE*, 21(5):34–41, Sep/Oct 2001.
- E. Reinhard, A.O. Akuyz, M. Colbert, C.E. Hughes, and M. O’Connor. Real-time color blending of rendered and captured video. *The Interservice/Industry Training, Simulation, and Education Conference I/ITSEC, Orlando, FL, (1502):1–9*, 2004.
- A. Shafer and D. Lischinski. Using color to separate reflection components. *Color Research and Application*, 10(4):210–218, Winter 1985.
- H. L. Shen and J. H. Xin. Transferring color between three-dimensional objects. *Applied Optics*, 44(10):1969–1976, 2005.
- S. Tominaga and B.A. Wandell. Standard surface-reflectance model and illuminant estimation. *Journal of Optical Society of America*, 6(4):576–584, April 1989.

- J. van de Weijer and R. van den Boomgaard. Least squares and robust estimation of local image structure. *IJCV*, 64(2-3):143–155, September 2005.
- R. van den Boomgaard and J. van de Weijer. On the equivalence of local-mode finding, robust estimation and mean-shift analysis as used in early vision tasks. *Proceedings ICPR*, August 2002.
- E. Vazquez, J. van de Weijer, and R. Baldrich. Image segmentation in the presence of shadows and highlights. In *ECCV '08: Proceedings of the 10th European Conference on Computer Vision*, 2008.
- A. V. Vezhnevets. Growcut - interactive multi-label n-d image segmentation by cellular. *Graphicon'2005 conference proceedings*, 2005.
- Y. Weiss. Deriving intrinsic images from image sequences. In *Computer Vision, 2001. ICCV 2001. Proceedings. Eighth IEEE International Conference on*, volume 2, pages 68–75, July 2001.
- X. Xiao and L. Ma. Color transfer in correlated color space. In *VRCIA '06: Proceedings of the 2006 ACM international conference on Virtual reality continuum and its applications*, 2006.